Synchrotron X-ray radiography studies of pitting corrosion of stainless steel: Extraction of pit propagation parameters

Ghahari, Seyed; Krouse, Donal; Laycock, Nicholas; Rayment, Trevor; Padovani, Cristiano; Stampanoni, Marco; Marone, Federica; Mokso, Rajmund; Davenport, Alison J.

DOI:
10.1016/j.corsci.2015.06.023

Corrosion Science 100 (2015) 23–35

Contents lists available at ScienceDirect

Corrosion Science

journal homepage: www.elsevier.com/locate/corsci

Synchrotron X-ray radiography studies of pitting corrosion of stainless steel: Extraction of pit propagation parameters

Majid Ghahari[a], Donal Krouse[b], Nicholas Laycock[a], Trevor Rayment[a,c], Cristiano Padovani[d,1], Marco Stampanoni[e,f], Federica Marone[e], Rajmund Mokso[e], Alison J. Davenport[a,*]

[a] College of Engineering and Physical Sciences, University of Birmingham, UK
[b] Callaghan Innovation, PO Box 31310, Lower Hutt 5040, New Zealand
[c] Diamond Light Source Ltd., UK
[d] Radioactive Waste Management Directorate, Nuclear Decommissioning Authority, UK
[e] Swiss Light Source, Paul Scherrer Institute, Switzerland
[f] Institute for Biomedical Engineering, University and ETH Zürich, Switzerland

ARTICLE INFO

Article history:
Received 24 March 2015
Received in revised form 11 June 2015
Accepted 15 June 2015
Available online 21 July 2015

Keywords:
A. Stainless steel
C. Pitting corrosion
C. Kinetic parameters
B. Galvanostatic
B. Potentiostatic
B. Electrochemical calculation

ABSTRACT

In situ synchrotron X-ray radiography was used to observe the evolution of 2D pits growing at the edge of stainless steel foils in chloride solutions of varying concentrations under current and potential control. A method was developed for measuring the local anodic current density along the perimeter of pits from the rate of advance of the pit into the metal. Pit depth tends to increase with time with kinetics consistent with diffusion control (under a salt layer), whereas lateral development (on film-free surfaces) is influenced by solution conductivity. Perforated covers formed on pits control their growth and stability.

1. Introduction

Stainless steels are employed in many industrial and architectural applications owing to their good corrosion resistance and other desirable properties. It is well known, however, that localised corrosion (and in particular pitting corrosion) can occur in the presence of halides (particularly chlorides). This form of damage can often lead to the degradation of both functional and cosmetic properties of components. In the presence of mechanical stresses, this form of damage has been observed to potentially lead to the development of stress corrosion cracks (SCC), thus degrading the structural properties of components (e.g. [1]).

The work described in this paper aims at further elucidating the nature of pitting propagation mechanisms in order to support the development of mechanistic models able to predict the likely extent and kinetic of damage in relevant conditions. Whilst relevant to many applications, the work was carried out with the specific aim of supporting the development of safety cases and long term strategies for the storage and disposal of radioactive waste in the UK (in particular intermediate level waste, ILW [2], which is currently packaged in stainless steel containers grades 304L and 316L).

It is well established that corrosion pits in stainless steel grow by an undercutting mechanism in which the pit maintains an overall hemispherical or dish shape covered by a perforated metal cover [3–13]. The fine structure is formed by local inhomogeneity in the current density in different regions of the pit, which has been simulated in a model developed by Laycock and co-workers for austenitic stainless steel (300 series) [14–17]. The model assumes that there are three different regions of a growing pit: the passive region near the mouth or lacy cover where the concentration of metal ions is low, a diffusion-limited region at the bottom where the pit is covered in a salt layer, and an actively dissolving region at the sides where there is neither passive film nor salt layer to limit dissolution. In this paper, radiographic measurements of 2D pits on

* Corresponding author.
E-mail address: a.davenport@bham.ac.uk (A.J. Davenport).
[1] Since April 2014 a wholly owned subsidiary of the Nuclear Decommissioning Authority, Radioactive Waste Management Ltd.

http://dx.doi.org/10.1016/j.corsci.2015.06.023

Table 1
$D_{eff}\Delta C$ values reported in literature obtained from 1D artificial electrode experiments all assuming $z = 2.2$.

$D_{eff}\Delta C$ ($10^{-8} \times$ mol cm^{-1} s^{-1})	Condition	Reference
3.57	$FeCl_2$ in water	Kuo and Landolt [20]
3.46	304 stainless steel, 1 M NaCl	Gaudet [21]
3.39	302 stainless steel, 1 M NaCl	Laycock and Newman [26]
3.95	304 stainless steel, 1 M NaCl	Ernst and Newman [11]
~2.5	316 stainless steel, 1 M NaCl	Carcea et al. [28]

stainless steel grades 304 and, to a lesser degree, 316 are used to test the assumptions made in the model and provide quantitative data on the inhomogeneous local current densities within growing pits.

It has long been assumed that pit stability is controlled by diffusion: in order to maintain an aggressive environment within the pit that prevents repassivation, the rate at which metal ions escape from the mouth of pits must be no greater than the rate at which they are produced by anodic dissolution processes [18]. Pit stability is thus usually described in terms of the pit stability parameter *i.x*, the product of the current density at the bottom of the pit *i* and the pit depth *x*. The critical value of *i.x*, which must be exceeded for a pit to remain stable, has been experimentally determined to be 3 [8,19] or 4 [9] mA/cm for stainless steel in chloride solutions. However, these parameters are generally determined from electrochemical measurements in which pits are assumed to grow in a hemispherical shape at a uniform current density. In order to develop models that more accurately reflect pit propagation, it is necessary to make direct measurements of the evolution of pit shape, and determine how the local current density varies within pits.

Artificial mono-dimensional (1D) pit electrodes have been previously used to develop an understanding of pit electrochemistry and dissolution kinetics [20–23]. These electrodes are usually pseudo-one-dimensional cavities with a small corroding surface area in which concentrated solutions of metal ions similar to a real pit are developed. These studies provide a basis for interpreting diffusion-limited current densities in 2- and 3-dimensional pits, which are the focus of this study. According to these studies, for pits growing under electrochemical conditions in which growth occurs under diffusion control, there is a relationship between (pit depth)^2 and time (using Faraday's second law in conjunction with Fick's first law for diffusion). In this approach, Fick's first law can be written as [23–25]:

$$i_{\lim} = \frac{zFD_{eff}\Delta C}{h} \quad (1)$$

where $i_{\lim}$ is the diffusion–controlled current density, z is the transferred charge (2.2 [26,27]), F is the Faraday constant, D_{eff} is effective diffusion coefficient, ΔC is the concentration gradient of metal ions at the pit bottom (or pit surface) and mouth (or bulk solution), and h is the pit depth. The relationship between pit depth and time is:

$$h^2 = \frac{MD_{eff}\Delta C}{\rho}t \quad (2)$$

where ρ is the metal density, M is the atomic mass and t is time. Therefore, for pits growing under diffusion control, the value of $D_{eff}\Delta C$ can be extracted from the slope in the plot of h^2 vs. growth time. The values of $D_{eff}\Delta C$ determined experimentally by a number of researchers are shown in Table 1.

Determination of the effective diffusion coefficient D_{eff} from $D_{eff}\Delta C$ requires knowledge of the concentration difference ΔC. It is generally assumed that the pit mouth has a metal ion concentration of zero. It is also assumed that pits growing in stainless steel under diffusion control are covered by a salt layer of $FeCl_2{\cdot}4H_2O$ [29], in equilibrium with a saturated metal-chloride solution. The saturated concentration of metal ions adjacent to the salt layer has been determined to be 3.5 M Fe^{2+}, 1.1 M Cr^{3+} and 0.5 M Ni^{2+} [30]. However, a saturation concentration of 4.25 ± 0.05 M for $FeCl_2$ reported by Kuo and Landolt [20] is commonly used as the concentration of metal ions at the pit bottom in the interpretation of 1D artificial pit measurements [8,21,26,31,32].

There have been relatively few attempts to observe and in some cases extract the average current density from video images taken of growing 2D pits. Frankel presented a method to directly measure the average anodic current density from the growing pit boundary velocity in Al [33], an Al alloy [34] and Ni–Fe [35] thin films. Subsequently, Ryan et al. [27,36] determined the anodic current density in pits propagating as 2D disks in stainless steel thin films by measuring the pit edge movement velocity. Ernst and Newman [11,12,37] studied stability of pit growth in detail and measured the kinetics of 2D pit propagation in depth and width and compared the results with kinetics in 1D pencil electrodes. They developed a semi-quantitative model for pit propagation which explained the lacy pit cover formation during the pit growth, although they did not measure current density within the pit. More recently, Tang and Davenport [38] tracked the pit boundary movement and computed the instantaneous but average current density in Fe-Co thin films. However, there have been no previous attempts to quantify the local current density during inhomogeneous growth of pits, although such local variation in current density has long been recognised [7].

In this paper, we present the use of synchrotron X-ray radiography to characterise the growth of 2D pits in a geometry similar to that previously used by Ernst and Newman [11,12], and extract the local current density around the perimeter of pits grown under both potentiostatic and galvanostatic conditions. The pit growth kinetics and stability are also studied. Further work [39,40] is being carried out to extend this information to the case of atmospheric conditions (particularly relevant to the management and disposal of radioactive wastes), in which concentrated solutions, cathodic processes and resistive (e.g. IR-drop) effects are likely to play an important role in the amount of damage associated with stainless steel pits over very long timescales (many decades).

2. Experimental method

2.1. Measurements

Pits were grown at the top edge of stainless steel foils (20 and 25 μm, Goodfellow Cambridge Ltd) cut to a width of ~0.7 mm embedded in epoxy resin (Araldite) and attached to an electrochemical cell as described in reference [41]. Grades 304 and, to a lesser degree, 316 were used in all experiments. Approximately 30 min prior to each measurement, the top edge of the foil was abraded with 4000 grit paper, washed, dried, and small drops of lacquer were applied to the two ends of the exposed surface to prevent pit initiation at the ends of the foil. This arrangement was generally effective in preventing the onset of crevice corrosion. In some experiments, pits growing underneath the lacquer were observed. The results of these measurements are described in a later section of this paper.

The electrochemical cell setup is described in detail in an earlier paper [41]. An Ivium (CompactStat) potentiostat was used to provide electrochemical control and all potentials were measured relative to an Ag/AgCl reference electrode ($[Cl^-] = 3$ M). Electrolytes were 0.005, 0.01, 0.1 and 1 M NaCl prepared from laboratory-grade chemicals and deionised water supplied from an Elix water

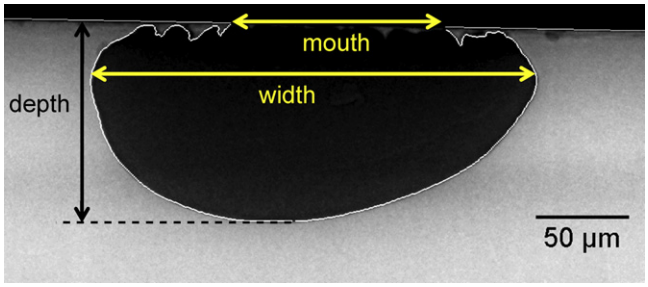

Fig. 1. Pit grown in 304 stainless steel foil at 650 mV vs. Ag/AgCl in 0.005 M NaCl after 470 s. The arrows indicate the definitions used for the pit "mouth", "width" and "depth".

purification system. All tests were performed at room temperature ($21 \pm 3\,^{\circ}C$) with the solution open to air.

The growth of pits was recorded through high resolution high speed X-ray radiography, carried out at 15 keV at the TOMCAT beamline at the Swiss Light Source (SLS). The TOMCAT detector, used with a 20× objective and 1 × 1 binning, covered a maximum field of view of 0.75 mm × 0.75 mm, providing the minimum pixel size of 0.37 μm × 0.37 μm. All radiographs were flat-field corrected before analysis.

Experiments typically lasted between 10 and 40 min. At high chloride concentrations, multiple pits typically initiated within seconds of applying the potential and grew simultaneously together. In these cases, experiments were short and terminated after two or more pits had merged together. However, at lower chloride concentrations, normally only one or two pits initiated or continued to grow. In lower chloride concentrations, the *induction time* for pits to initiate was longer [42]. Therefore, these experiments were performed for longer periods.

Pit parameters were automatically extracted from radiographs using a customised filter plug-in implemented into the ImageJ software [43], which is described elsewhere [41,44]. Details of the extraction of the local current density are described in reference [44].

2.2. Pit edge detection and definition of pit depth and width

In order to quantify the growth of pits during successive radiographs, it is necessary to extract the co-ordinates of the pit boundary as well as parameters associated with the pit morphology. Fig. 1 illustrates the definitions used in this work for the pit "depth", "width" and "mouth". The maximum distance from pit bottom up to foil interface with solution is defined as the pit "depth", the maximum lateral extent of pit is defined as pit "width", and the horizontal distance between the two points where pit boundary connects to the foil top surface is considered as pit "mouth" (or the distance between the junction points of pit internal perimeter with foil interface with solution).

2.3. Current density extraction

Once the pit boundary has been defined for several successive radiograph frames of a growing pit, then the local current densities at the pit boundary can be calculated from the boundary velocity. Fig. 2 shows the position of the pit boundary 20 s later than its earlier position (yellow boundary).

The velocity of the pit boundary can be calculated at each point by the displacement along the local normal from one frame to a subsequent one at a later time dt. The displacement is measured by the normal distance from the centre of two adjacent points in the boundary at time t with respect to the boundary at time $t + \mathrm{d}t$.

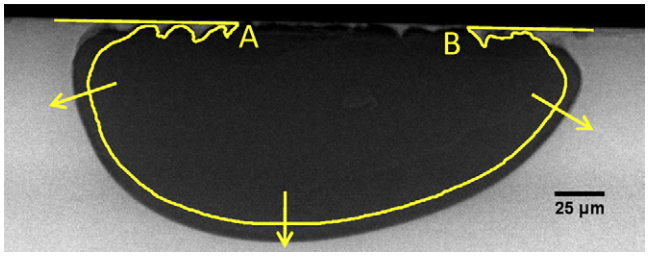

Fig. 2. Movement of the pit boundary after 20 s compared with its earlier position (yellow boundary). (For interpretation of the references to color in this figure legend, the reader is referred to the web version of the article.)

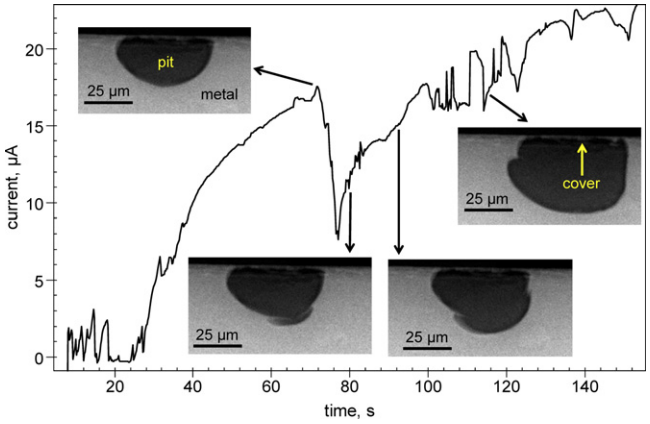

Fig. 3. Variation of pit current with time in a potentiostatic measurement carried out on 304 at 650 mV (Ag/AgCl) in 0.005 M NaCl solution, together with radiographs showing the appearance of the pit at different times; the current increases as the pit grows and periodically drops due to perforation of the cover and local passivation.

The velocity is then converted using Faraday's 2nd law into a local current density:

$$i = \frac{\mathrm{d}x}{\mathrm{d}t}\frac{zF\rho}{M} \tag{3}$$

where i is the local current density, dx/dt is the local measured pit boundary velocity.

3. Results

3.1. Characteristic pit growth behaviour

The typical variation with time of the pit current measured in a potentiostatic experiment on 304 (650 mV (Ag/AgCl) in 0.005 M NaCl), together with images showing typical radiographs collected at different times are shown in Fig. 3. It can be seen that, after a period of initiation, the current generally increases approximately according to $t^{1/2}$ but strong fluctuations are imposed upon this trend. The radiographs also show that a dish-shaped pit with a very thin perforated metal cover gradually grows through period of relatively fast local growth followed by a decrease in growth rate and eventual passivation of some of the (previously active) surfaces, accompanied by the development of fast growing regions ('lobes'), generally growing sideways. As the pit grows, the supplied current increases owing to the increase in pit surface area. However, at ~70 s, there is a sudden drop in current. This is likely to be associated with development of a new perforation that allows escape of metal ions from the pit, diluting the pit solution and leading to local passivation. At ~75 s, the current starts to increase again: this is associated with lateral growth of a new region of attack at the bottom of the pit. The continuing current fluctuations are a consequence of ongoing perforation and development of new regions of

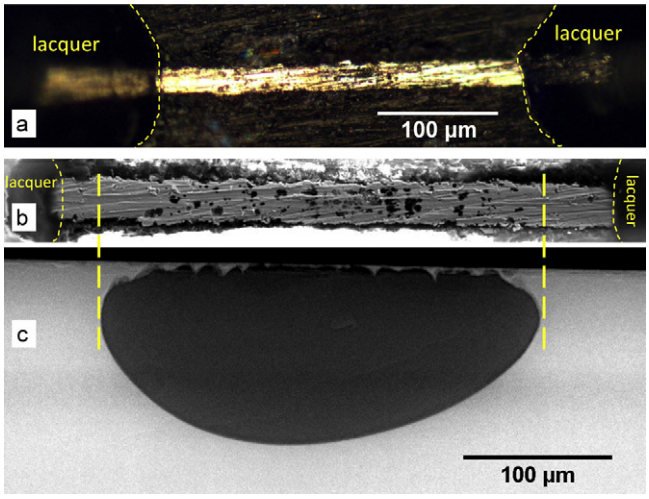

Fig. 4. The pit shown in Fig. 3 following growth for 600 s at 650 mV vs. Ag/AgCl in 0.005 M NaCl; (a) optical micrograph of top surface of the foil, (b) higher magnification SEM image of the top of the foil showing the perforated cover, (c) radiograph of the final shape of pit. The scale bar for (b) and (c) is identical. The yellow dashed lines correlate the pit width in (b) and (c). The dark regions at both edges of foil in (a) and (b) are the lacquer/epoxy coating placed to protect edges of foil from pit/crevice intiation.

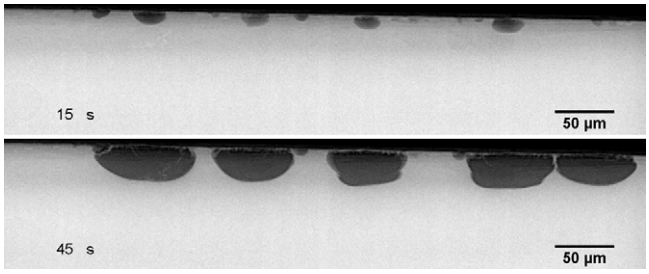

Fig. 5. Radiographs of several 2D pits growing under potentiostatic control at the edge of a 20 μm foil of 304 stainless steel in 0.1 M NaCl at +650 mV vs. Ag/AgCl. The time at which each radiograph was taken is shown (the potential was applied at $t = 0$).

lateral pit growth, leading to the characteristic "lacy" perforated pit cover shown in Fig. 4. Pit covers of this type have previously been observed for pits in stainless steels [3,4,6–9,45]. Fig. 4 also shows an optical micrograph indicating the location of lacquer drops at the two ends of the foil that were applied to prevent pit initiation.

3.2. Pit growth under potentiostatic and galvanostatic control

In this study, under potentiostatic control and in concentrations of 0.1 M NaCl and above, multiple adjacent pits of similar size and shape were formed on grade 304, which grew together until they merged (Fig. 5). This simultaneous initiation and propagation of multiple pits appears to be a characteristic feature of potentiostatic control, since, in these conditions, there is no limit to the current that can be supplied to the system. A video of this process (10× times speeded up) is provided in the online version of this article (Video 1).

Supplementary material related to this article can be found, in the online version, at doi:10.1016/j.corsci.2015.06.023.

Conversely, it was found to be difficult to initiate pits reproducibly under galvanostatic conditions due to competing crevice corrosion at the edge of the foil that was in contact with epoxy. Therefore, in this work, galvanostatic measurements were generally preceded by a brief period under potentiostatic control to initiate the pits. Fig. 6 shows typical growth of a pit grown in

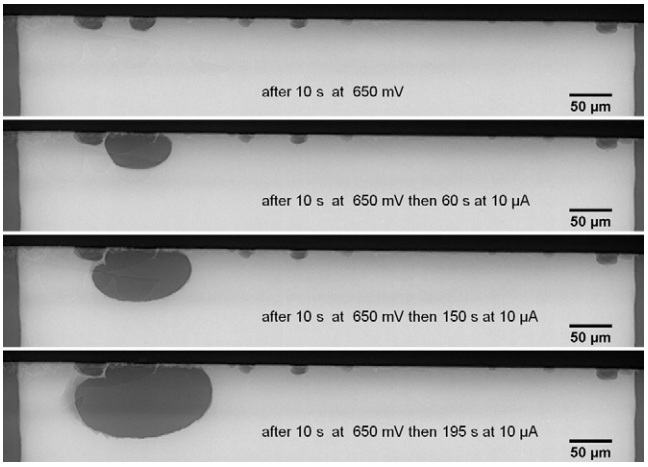

Fig. 6. A series of radiographs of a 2D pit growing at the edge of 20 μm foil of 304 stainless steel that was initiated in 0.1 M NaCl at +650 mV (Ag/AgCl) for 10 s then propagated galvanostatically at 10 μA. The time at which each radiograph is taken is shown (+650 mV (Ag/AgCl) was applied at $t = 0$).

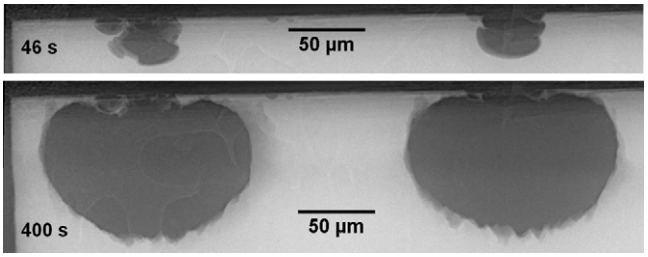

Fig. 7. Radiographs of two pits growing simultaneously at the edge of 20 μm foil of 304 stainless steel in 0.01 M NaCl at 20 μA after initiation at 650 mV vs. Ag/AgCl for 10 s.

galvanostatic conditions at a current of 10 μA, following pit initiation under potentiostatic control at +650 mV (Ag/AgCl) for a period of 10 s. Further information on the current signal during growth of pits of this type is provided elsewhere [41,44] and a video of this process (10× times speeded up) is provided in the online version of this article (Video 2). It is evident that a number of pits were initiated in the potentiostatic regime, but once the sample was switched to galvanostatic control, the smaller pits repassivated and only one pit survived and continued to grow. It was always the case in the galvanostatic measurements carried out in this way that only one or two pits survived after switching from potential control to current control. Following a switch to galvanostatic control, if two pits survived, they usually grew at the same rate and to the same size as illustrated in Fig. 7. A video of this process (10× times speeded up) is provided in the online version of this article (Video 3). Further evidence illustrating pit survival following switching from potential control to current control is available in reference [44].

Supplementary material related to this article can be found, in the online version, at doi:10.1016/j.corsci.2015.06.023.

3.3. Pit morphology

A difference in morphology was frequently observed between pits grown under potentiostatic vs. galvanostatic control. Fig. 8 compares the morphology of pits grown potentiostatically and galvanostatically after a charge of ~2.6 mC has passed. The potentiostatically grown pit (Fig. 8(a)) is shallow and smooth with a clearly defined and smooth perimeter. In contrast, the galvanostatically grown pit (Fig. 8(b)) is deeper but has a rougher surface and an etched perimeter.

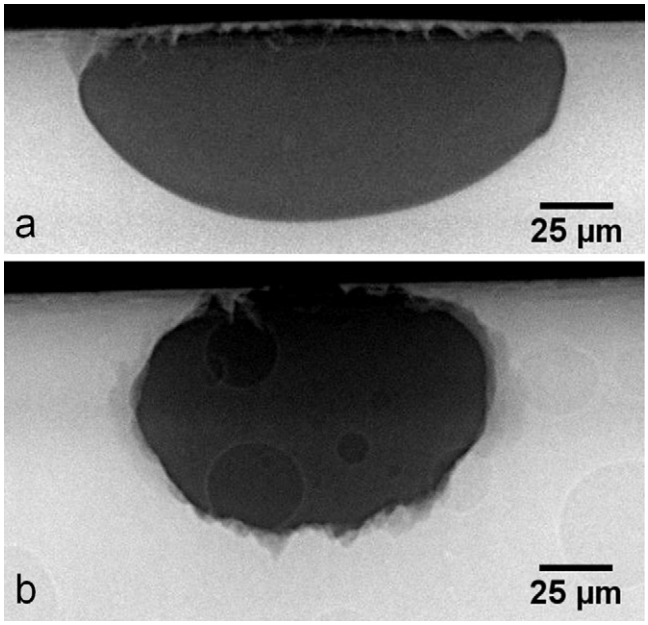

Fig. 8. Radiographs of 2D pits grown at the edge of 20 μm foil of 304 stainless steel in 0.01 M NaCl until a charge of ~2.6 mC had been passed; (a) potentiostatic growth at 600 mV (Ag/AgCl) for 220 s, (b) galvanostatic growth at 10 μA for 300 s after 10 s initiation at 650 mV vs. Ag/AgCl.

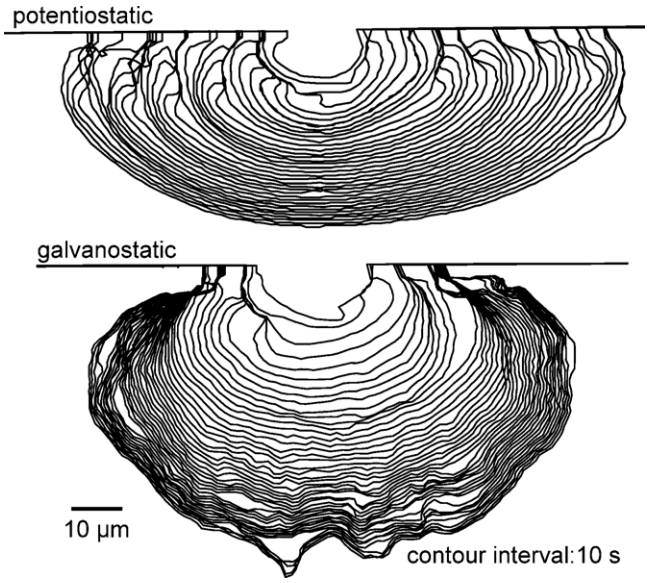

Fig. 9. Pits grown in 0.01 M NaCl potentiostatically at 550 mV (Ag/AgCl) and galvanostatically at 10 μA for 450 s. Counters at 10 s interval.

It should be noted that in this work, the potentials that were applied under "potentiostatic" control and observed under "galvanostatic" control were significantly different. For example, the measured potential decays from 650 mV to 150–200 mV (Ag/AgCl) within a period of 150 s following the switch from potential control to an applied current of 10 μA. It is therefore likely that the observed differences can be attributed to the difference in interfacial potential.

Fig. 9 shows the boundaries of pits at different stages of growth for potentiostatic and galvanostatic pits. In the pit grown potentiostatically (at higher potential), sideways growth via propagation of lateral lobes can be observed. However, more uniform growth in all directions towards a circular shape can be observed for the galvanostatically grown (low potential) pit.

3.4. Effect of lacquer on pit shape

In these experiments, lacquer was applied to the ends of the metal foil to prevent pit initiation and increase the probability of growth of a single pit in the centre of the foil (Fig. 10(a)). However, sometimes a pit that initiates in the centre of the foil may grow under the lacquer (Fig. 10(b–d)). The presence of the lacquer means that perforation of the pit cover does not lead to local dilution of the pit solution. Instead, the pit is able to continue to grow horizontally, as shown in the left side of Fig. 10(b) and the right side of Fig. 10(c and d). The other side of each pit grows by the mechanism of successive perforation. This indicates how partially covered pits may lead to development of crevice corrosion.

3.5. Local current densities within pits

Fig. 11 shows a growing pit with a plot of local current density along the pit boundary measured from the velocity of boundary movement by considering frames that are 5 s apart. In this graph (as in the following ones), the abscissa in the plots of current density associated with different images represent the distance of a line traced across the pit contour (i.e. the pit boundary) from the point on the left-hand side of the image in which the pit intersects the original surface, which enables location of different points on the pit boundary through a single coordinate. The developing fronts within the pits and their corresponding current density in the plot are marked with X and Y. At all of the times illustrated in Fig. 11, it can be seen that towards the outermost points on the perimeter of the pit, the current density drops to zero, which is to be expected for a passive region of the electrode. The transition from passive to active surface is abrupt leading to undercutting and lobe formation. In the centre of the dissolving surface (i.e. at the bottom of the pit) the current is constant, generating a local minimum between two regions of maximum dissolution (located on the side).

Figs. 12 and 13 show the time-dependence of local current densities within the pits. At each frame time, the maximum current density along the pit perimeter was extracted. Also, the current density at the mid-point of the pit was extracted in order to give an indication of the current density at the pit bottom, assuming the symmetry of the pit cavity is retained during growth. The fluctuation in maximum current density illustrates the dynamic nature of growth at the developing lobes. It is evident that the current density values remain fairly constant for the pit growing under potentiostatic control (Fig. 12), whereas the current density decays during growth of the pit under galvanostatic control, following the gradual decrease in potential (Fig. 13).

Fig. 14 compares the maximum current density along the boundary of pits grown at 650 mV (Ag/AgCl) at different chloride concentrations of bulk solutions. A slight increase is observed in the maximum current density as the concentration of bulk chloride increases; this is likely to be associated with the lower IR drop in solution at higher concentrations leading to a higher interfacial potential.

3.6. Pit growth rate

In order to extract the pit growth parameter $D_{eff}\Delta C$, pits were grown for an extended period under potentiostatic control until they merged into a 1D pit. Fig. 15 shows a series of images at different times for pit grown in 1 M NaCl at 650 mV (Ag/AgCl). It can be seen that the coalescence of individual pits is relatively rapid, and by 300 s there is a uniform dissolution front and no pit cover is evident. It should be noted that it was not possible to grow

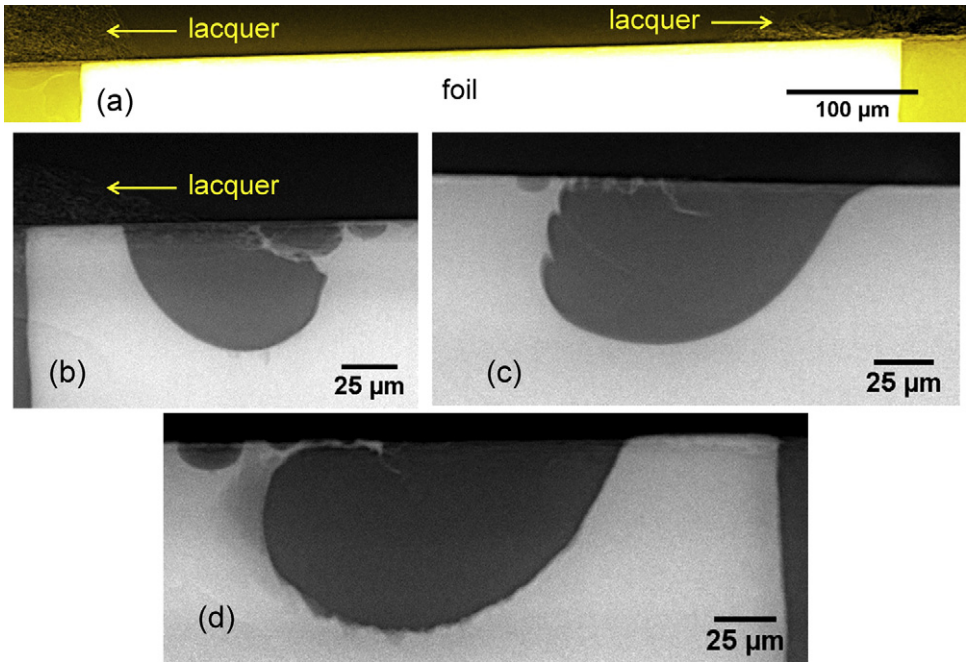

Fig. 10. (a) and (b) Lacquer covering the foil top interface with the epoxy to prevent pit/crevice intiation at the edges. (b)–(d) Pit growth morphology where one side is covered with lacquer for pits grown in 0.1 M NaCl at (b) 650 mV (Ag/AgCl) for 10 s then 183 s at 20 μA (lacquer on left side), (c) 650 mV for 10 s, 550, 450 and 350 mV (Ag/AgCl) each for 60 s (lacquer on right side), and (d) 650 mV (Ag/AgCl) for 10 s following 20 μA for 300 s (lacquer on right side).

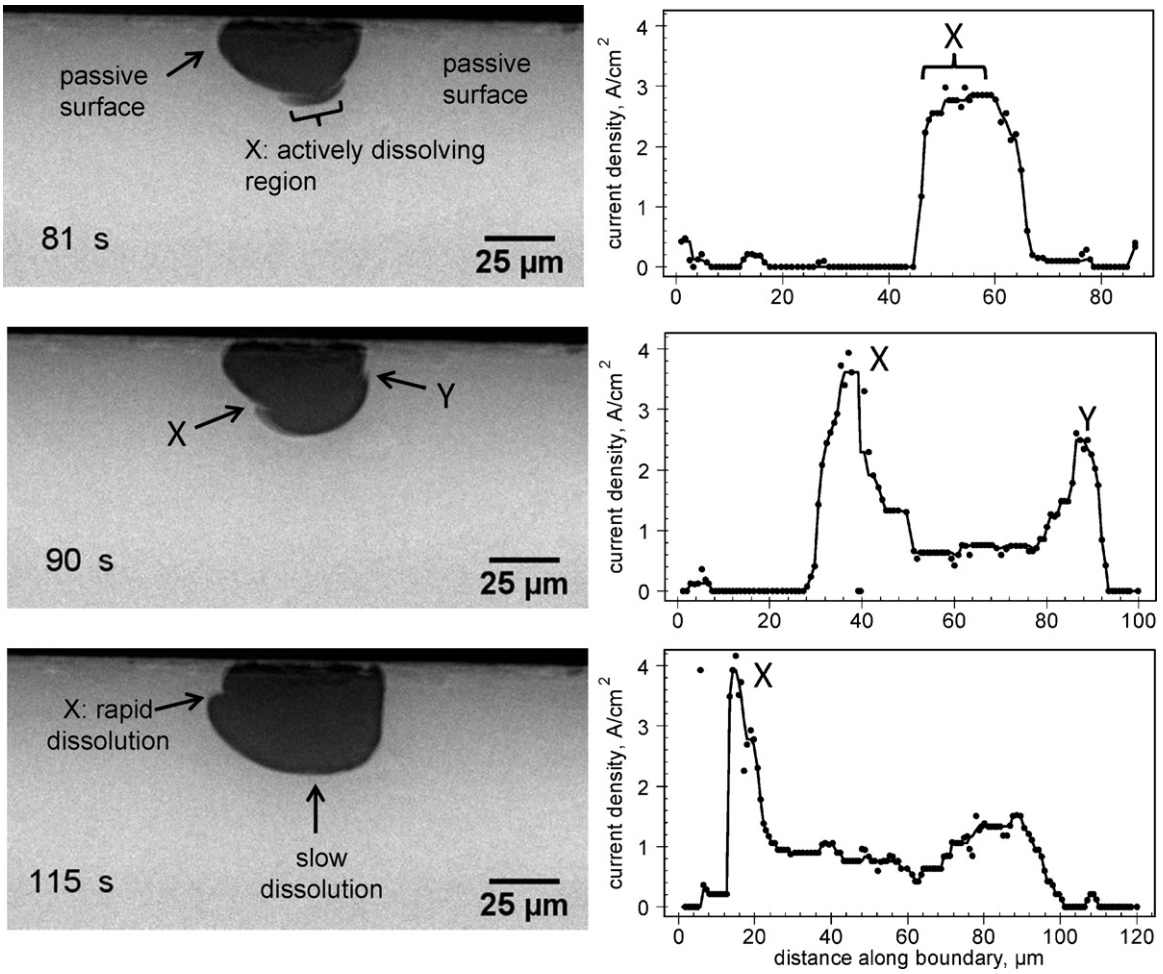

Fig. 11. Sequential growth of a pit and corresponding local current density along the pit boundary measured from the velocity of boundary movement by considering frames that are 5 s apart. X and Y are developing fronts within the pits and their corresponding current density in the plot.

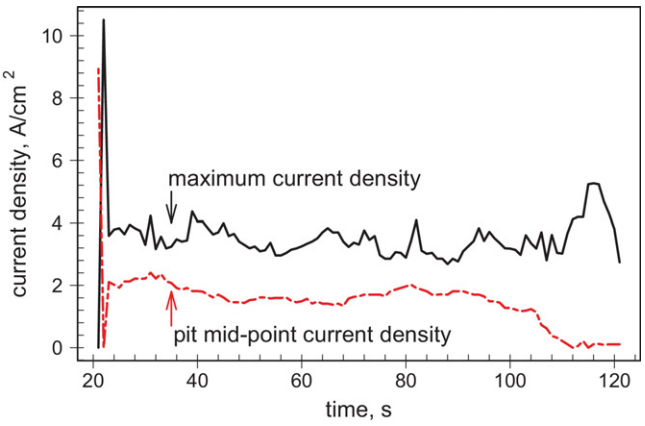

Fig. 12. Maximum and pit mid-point current density along pit boundary as a function of time during growth of the pit grown on 304 stainless steel foil in 0.1 M NaCl at 650 mV vs. Ag/AgCl.

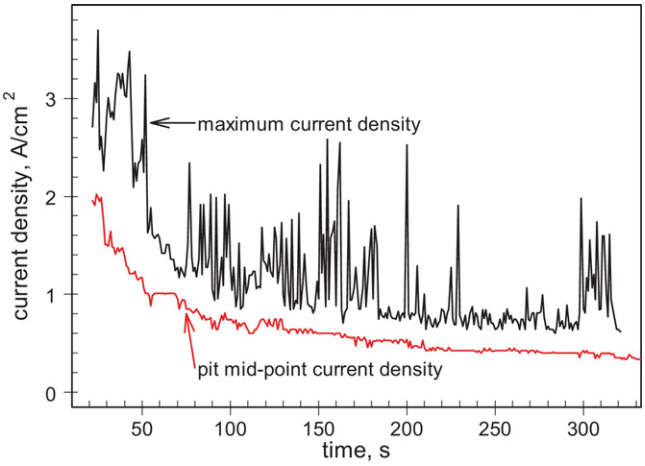

Fig. 13. Maximum and pit mid-point current density along pit boundary as a function of time during growth of the pit grown on 304 stainless steel foil in 0.1 M NaCl at 10 μA following initiation at 650 mV (vs. Ag/AgCl) for 10 s.

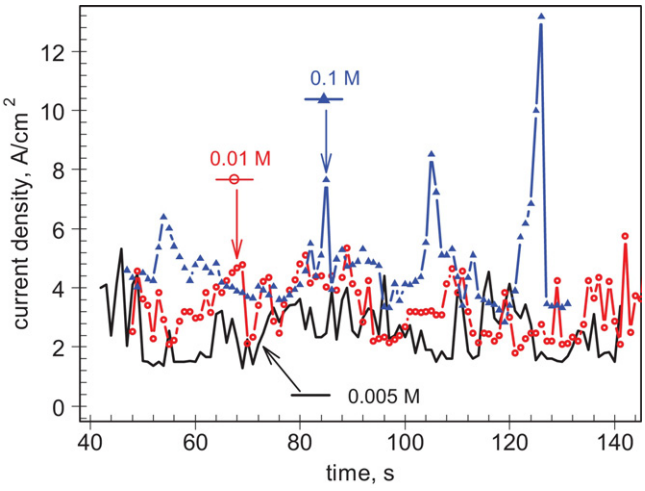

Fig. 14. Maximum current density along pit perimeter grown at 650 mV (Ag/AgCl) at different bulk chloride concentration.

individual pits of any size in 304 in 1 M NaCl under these experimental conditions.

Fig. 16 shows a graph of pit depth squared against time for the pit shown in Fig. 15. The depth values are taken from the

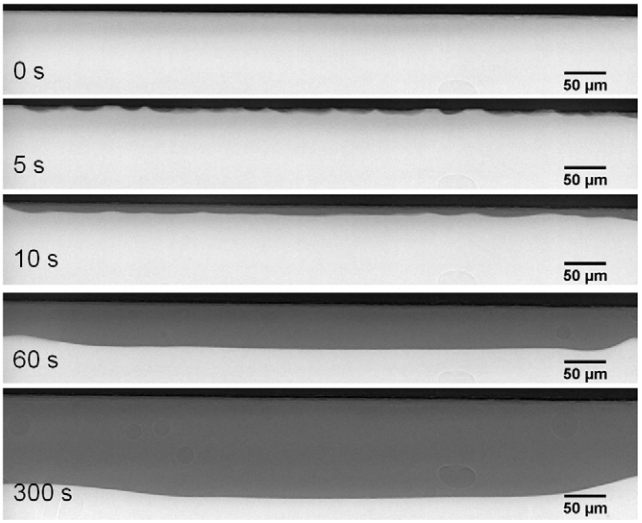

Fig. 15. Pit growth stages on a 304 stainless steel foil at 650 mV vs. Ag/AgCl in 1 M NaCl, leading to the formation of a 1D pit; shallow dish-shaped micropits initiate all along the surface (still at 5 s) and merge together (still at 10 s). General dissolution continues for the rest of experiment (shown up to 300 s). The maximum vertical distance from the pit bottom up to the mouth (original interface between foil and solution) is considered as the pit depth.

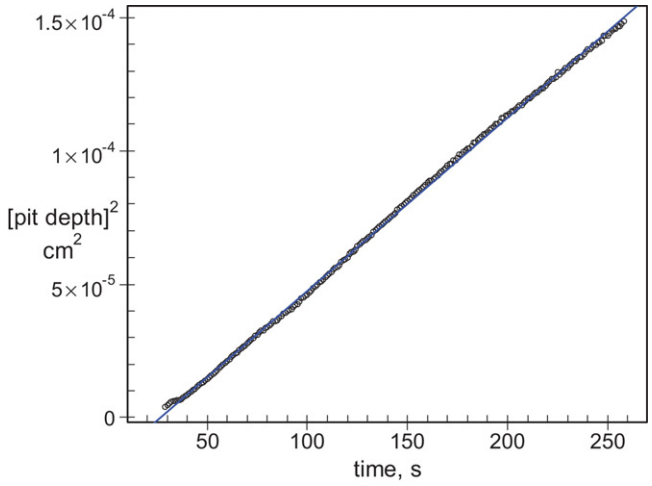

Fig. 16. Pit depth squared as a function of time for the pit shown in Fig. 15 (1D pit grown on 304 stainless steel foil at 650 mV (Ag/AgCl) in 1 M NaCl), in which generalised dissolution occurs after multiple pits have coalesced. The pit depth values are taken from the deepest part of the pit.

deepest part of the pit up to the pit mouth (original interface between foil and solution). It can be seen that the plot is linear to a good level of approximation. Taking into account Eq. (2) and considering $M = 57.6\,\mathrm{g\,mol^{-1}}$ and $\rho = 7.82\,\mathrm{g\,cm^{-3}}$, from the gradient of the plot, the value of $D_{eff}\Delta C$ is estimated to be $4.36 \times 10^{-8}\,\mathrm{mol\,cm^{-1}\,s^{-1}}$.

The same approach described above was used in other measurements leading to the propagation of isolated '2D' pits; in this case it was assumed that if the resulting plot of (pit depth)^2 against time was linear, then the dissolution is diffusion controlled and diffusion length is equal to the pit depth.

An example of this methodology is reported in Fig. 17, which shows an example of an isolated (2D) pit grown on a 316L stainless steel foil in 1 M NaCl at 750 mV (Ag/AgCl). In general, in the electrochemical conditions tested, pit growth on 316L was more difficult and less reproducible than for 304, but this experiment shows a good example illustrating the growth of a pit with

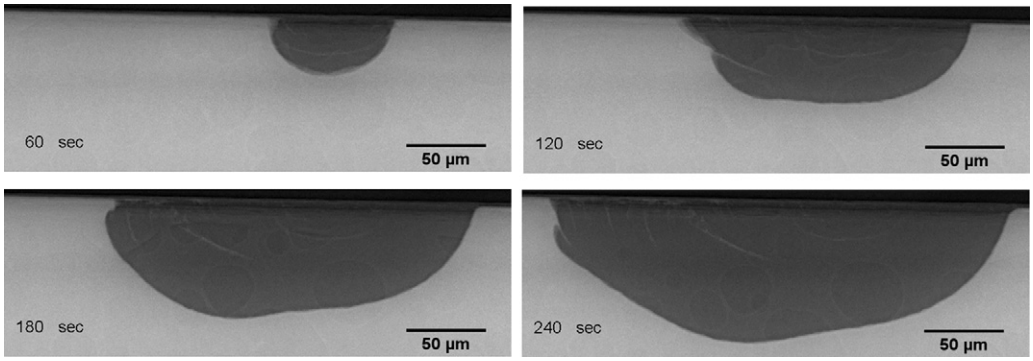

Fig. 17. Pit growth in a 316L stainless steel foil at 750 mV vs. Ag/AgCl in 1 M NaCl.

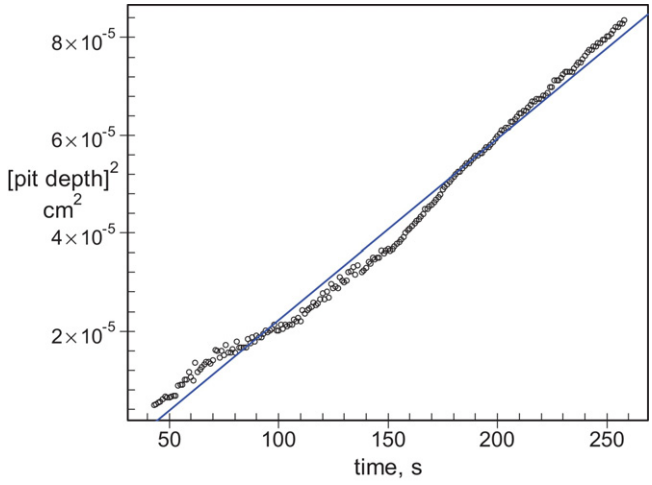

Fig. 18. (Pit depth)^2 as a function of time for a 2D pit formed on 316 in 1 M NaCl at 750 mV vs. Ag/AgCl (the pit shown in Fig. 17).

relatively little cover. A plot of pit depth squared as a function of time is shown in Fig. 18. The linear correlation between the square of the depth and time suggests that the pit is growing under diffusion control. In this measurement, the value of $D_{eff}\Delta C$ was estimated to be 2.5×10^{-8} mol cm^{-1} s^{-1}.

Table 2 summarises the $D_{eff}\Delta C$ values obtained for pits under different conditions. It may be seen that the $D_{eff}\Delta C$ values obtained for all 2D pits are lower than the values measured for the 1D pit. Aside from this, the values are relatively similar across measurements performed in potentiostatic conditions at different chloride concentrations, with higher variability in measurements carried out at lower chloride concentrations (pits No. 19–23). Slightly lower values are obtained for galvanostatically grown pits (No. 24–30), with relatively little variation. This variation can be attributed to the variation in the degree of perforation of the pit cover. Therefore, a "perforation factor" was estimated for 2D pits by taking the ratio of the value of $D_{eff}\Delta C$ for a 2D pit and that of the 1D pit.

Fig. 19 compares pits grown for ca. 60 s after initiation in (a) 0.005 and (b) 0.1 M NaCl under potentiostatic conditions (650 mV vs. Ag/AgCl). At a concentration of 0.1 M, under potentiostatic control, pits normally grew in a dish-shaped or semi-elliptical form. In more dilute solutions (0.01 and 0.005 M), pits grew narrower and deeper. This is illustrated in Fig. 20, which shows the evolution of pit width with depth for different chloride concentrations. These plots are approximately linear for pits less than ca. 60 μm depth, from which it may be deduced that the ratio of pit width to pit depth is approximately constant for early stages of growth. At later stages, the slope of the curve increases, indicating a relative increase of the rate of propagation with width in respect to depth. The overall ratio of width to depth increased with chloride concentration from ca. 1–2 in 0.005 M NaCl to ca. 4 in 0.1 M NaCl, indicating a faster growth sideways than with depth.

Fig. 21 compares the width and depth of pits grown under constant potential of 650 mV (Ag/AgCl) or current of 10 μA. At both conditions, the pit width increases with the increase in bulk chloride concentration. For a given concentration, pits are wider under potential control than under current control (Fig. 21(a)). However, as mentioned above, this is a likely to be the result of the significant difference between the potential of the two electrochemical regimes, e.g. 200 s after growth, the measured potentials of galvanostatically grown pits were ~140 and 208 mV (Ag/AgCl) at 0.1 and 0.01 M, respectively.

The pit growth in depth does not show systematic dependence on applied current, potential or chloride concentration (Fig. 21(b)).

3.7. Pit stability product

A value for the pit stability product can be calculated from the product of the local current density (i_a) and the local depth at each point along the pit surface. It is assumed that the local depth may be defined as the vertical distance from the pit surface up to the pit rim. Fig. 22 shows the stability product along the boundary of the pit grown in 0.1 M NaCl at 10 μA for 22 and 47 s following initiation at 650 mV (Ag/AgCl) for 10 s. At the initial stages (a) the stability product is less than 2.5 mA/cm all along the pit boundary. As the

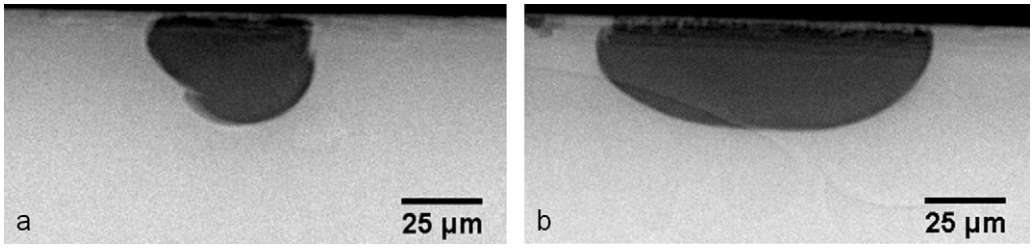

Fig. 19. Pits initiated and grown for ca. 60 s at 650 mV vs. Ag/AgCl reference electrode in (a) 0.005 M and (b) 0.1 M NaCl.

Table 2
$D_{eff}\Delta C$ calculated for pits grown in different conditions. The pit reported in the 1st row is a '1D pit' (general dissolution of the entire exposed surface), while the other experiments all refer to '2D pits' (grown in isolation from each other and leading to damage only locally). All pits were grown in 304 foil, unless otherwise stated.

No.	[NaCl] (M)	E (mV)[a]	I (μA)[c]	$D_{eff}\Delta C \times 10^8$ (mol cm^{-1} s^{-1})	Perforation factor (%)[e]	Notes
1	1	650		4.360	100	1D pit, uncovered[f]
2	1	750		2.509	58	316L SS, single pit
3	0.1	650		2.074	48	3,4[b]
4	0.1	650		1.919	44	3,4[b]
5	0.1	650		2.296	53	One of two pits[d]
6	0.1	650		2.023	46	6,7,8[b]
7	0.1	650		2.058	47	6,7,8[b]
8	0.1	650		1.874	43	6,7,8[b]
9	0.1	650		1.052	24	9–12[b]
10	0.1	650		1.799	41	9–12[b]
11	0.1	650		1.986	46	9–12[b]
12	0.1	650		2.288	52	9–12[b]
13	0.1	650		2.661	61	One of two pits[d]
14	0.1	650		1.684	39	14–18[b]
15	0.1	650		1.655	38	14–18[b]
16	0.1	650		2.282	52	14–18[b]
17	0.1	650		2.182	50	14–18[b]
18	0.1	650		2.116	49	14–18[b]
19	0.01	650		3.749	86	One of two pits[d]
20	0.01	550		3.555	82	Single pit
21	0.01	600		0.832	19	Single pit
22	0.005	650		1.790	41	Single pit
23	0.005	650		4.110	94	[b]
24	0.1		50 μA	2.296	53	One of two pits[d]
25	0.1		10 μA	1.590	36	Single pit
26	0.1		10 μA	1.775	41	Single pit
27	0.1		20 μA	1.600	37	One of two pits[d]
28	0.01		10 μA	1.534	35	One of two pits[d]
29	0.01		20 μA	1.499	34	One of two pits (other pit No. 30)
30	0.01		20 μA	1.512	35	One of two pits (other pit No. 29)

[a] Potentiostatic mode: E (mV vs. Ag/AgCl).
[b] Multiple pits from same experiment (all pits in same experiment listed).
[c] Galvanostatic mode: pit initiated under potentiostatic conditions at 650 mV (Ag/AgCl) for 10 s and then grown at the current indicated I (μA).
[d] Other pit growing under resin.
[e] The "perforation factor" was estimated for 2D pits by taking the ratio of the value of $D_{eff}\Delta C$ for a 2D pit and that of the 1D pit (No. 1).
[f] Isolated (2D) pits could not be grown in 304 in this condition.

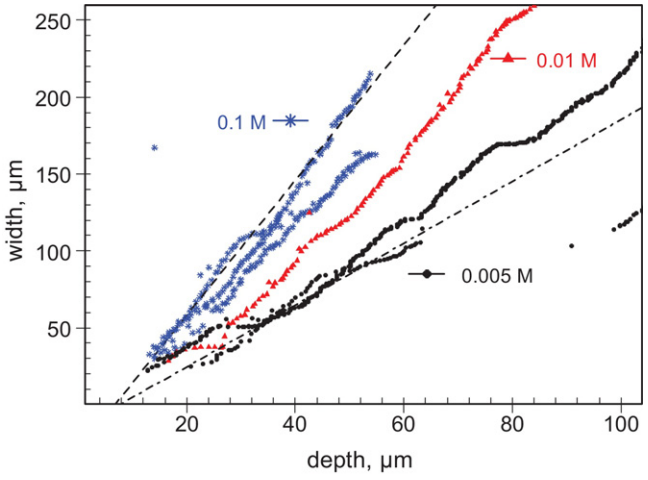

Fig. 20. Pit width against pit depth of pits grown potentiostatically at 650 mV vs. Ag/AgCl in NaCl solutions with the concentrations indicated.

pit grows, the stability product exceeds 3 mA/cm only at the pit bottom areas and fluctuates around this value during the rest of growth time. This value is broadly consistent with previous work [8].

Fig. 23 shows the maximum stability product as a function of time for galvanostatically grown pits at 10 μA in 0.1 M NaCl solutions. The stability products tend to fluctuate between 3 and 4 mA/cm with some sudden increases to higher values.

4. Discussion

4.1. Pit growth shape

It is evident from this work (Figs. 5 and 6) that both the shape and numbers of pits are influenced by whether the sample is under potentiostatic or galvanostatic control. Under potentiostatic growth conditions, multiple pits initiate and continue to grow at same rate (Fig. 5). This is consistent with the observation of the sudden initiation of pit sites and stable growth of pits above E_{pit} and the critical pitting temperature (CPT) [46,47].

In the experiments shown here, it was difficult to initiate pits reliably under galvanostatic control, so pits were initiated under potentiostatic control for 10 s and then grown under galvanostatic conditions. In similar conditions, it was previously found that all of the pits rapidly die except one "champion pit" [48,49]. The difference is that for galvanostatic growth, the amount of current is limited while the pit and thus dissolving surface area is growing larger, leading to a gradual decrease in current density. Under such conditions, the current flowing is insufficient to maintain a concentrated solution within pits, so they gradually repassivate.

If multiple pits are present initially, once the electrochemical control is switched to galvanostatic, the applied current will flow into the pits which provide the least electrical resistance (i.e. resistors in parallel according to conventional rules of electrical circuits). Therefore, only pits with lower electrical resistance may continue to grow. The electrical resistance may be mainly affected by the extent of pit active surface area and perforation of the lacy cover.

Fig. 9 compares the pit development mechanism under potential and current control. Under potential control, a pit propagates

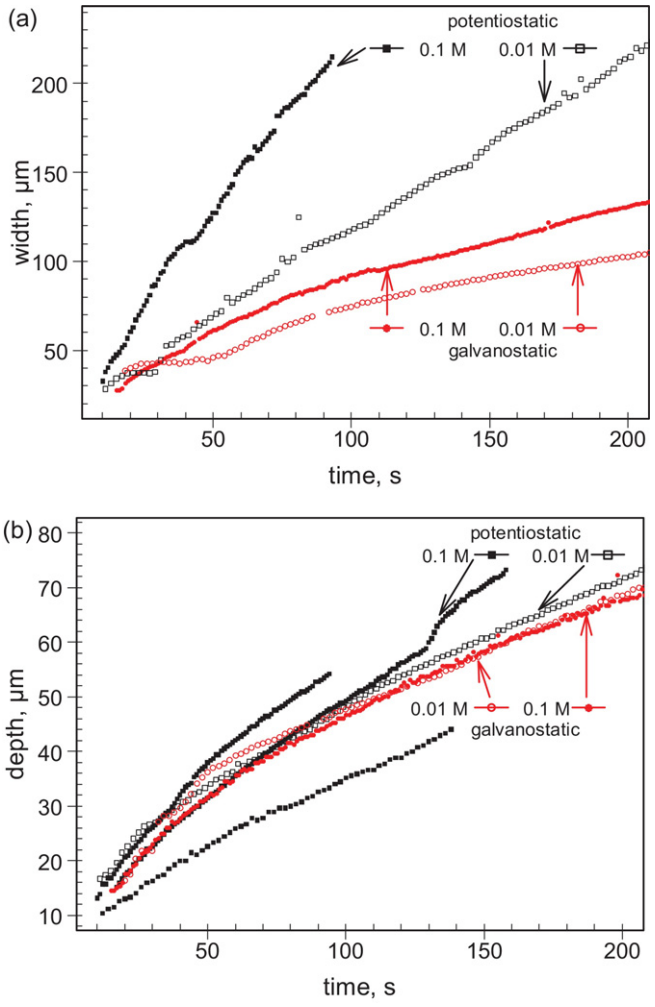

Fig. 21. (a) Width and (b) depth as a function of growth time for pits grown potentiostatically at a potential of 650 mV vs. Ag/AgCl or galvanostatically current of 10 μA in NaCl solutions of the concentrations indicated.

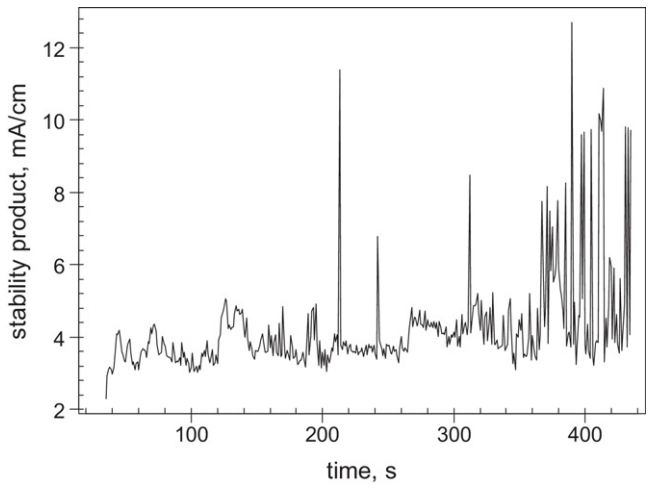

Fig. 23. The maximum pit stability product (for each frame) as a function of time for pit grown on 304 stainless steel foil in 0.1 M NaCl at 10 μA following initiation at 650 mV (Ag/AgCl) for 10 s.

by successive development of laterally expanding lobes consistent with the schematic model proposed by Ernst and Newman [11]. Pits growing under galvanostatic conditions initially propagate in a similar shape to potentiostatically grown pits; small lobes from both sides of the pit undercut metal and perforate the cover with a sharp pit perimeter. However, the pit shape gradually adjusts to accommodate the limited applied current with the lowest electrical resistance, resulting in a relatively uniform dissolution rate in all directions, thereby approaching an approximately circular shape. The ratio of pit width vs. pit depth is ca. 2–4 in the potentiostatically grown pits and ca. 1.4–2 in the galvanostatically grown pits, suggesting that pits grown under potentiostatic control tend to be less penetrating (more dish-shaped) than those grown under galvanostatic control (this may be related to the different potentials involved).

As the pit grows (galvanostatically) and its perimeter increases, the average current density and accordingly the interfacial potential decreases and the pit perimeter at the bottom transforms to a rough and etched surface. This transition agrees with Sato's idea [50,51] and the observations of Ryan et al. [27] that pits initiated at high potential often grow with a polished surface but if the potential

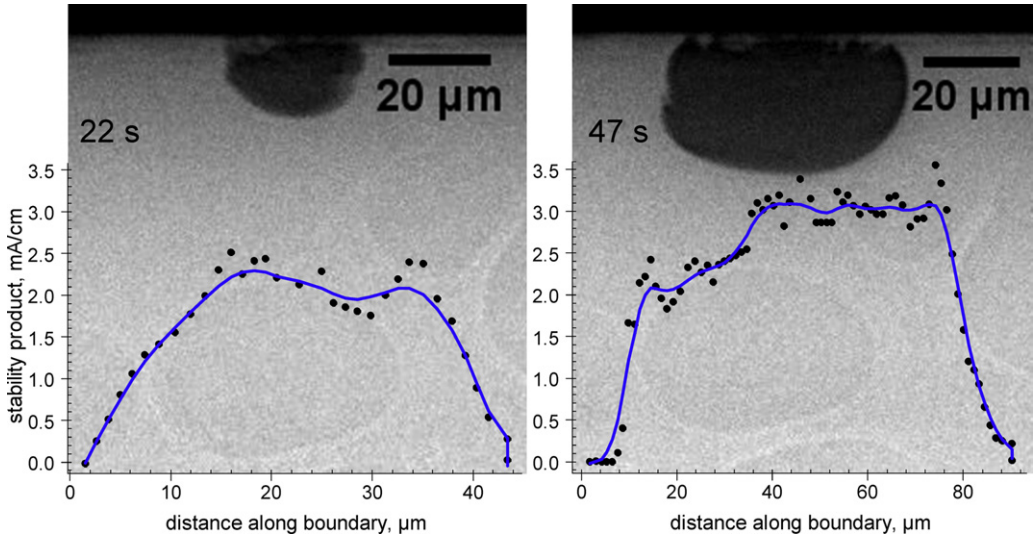

Fig. 22. Radiograph and local stability product along the perimeter of the pit grown on 304 stainless steel foil in 0.1 M NaCl at 10 μA for (a) 22 and (b) 47 s following initiation at 650 mV (Ag/AgCl) for 10 s.

is decreased, pits either repassivate or propagate in a salt layer-free active state with convoluted structure and lowest metal ion concentration possible for continuation of propagation.

In contrast, in pits grown under potentiostatic control, the pit perimeter looks sharp and well-defined during the whole growth period (see e.g. Figs. 4 and 5); this is consistent with observations of Sato [50,51] that pits grown at higher potentials have polished and bright internal surfaces, suggesting that they are covered by salt layer over the majority of their internal surface since polished surfaces are characteristic of electropolishing dissolution beneath salt [3,8,15,52]. Evidence for the presence of a crystalline salt layer at the bottom of pits has also been observed in X-ray diffraction measurements of 2D pits of the type shown in the present work [53].

It should be noted that in the present work, the potentiostatic measurements used a relatively high potential (+550 to +750 mV (Ag/AgCl)) whereas the galvanostatically grown pits develop at lower potentials (typically ranging from +600 down to <100 mV (Ag/AgCl)) during the growth of a pit). Thus, a significant difference in the evolution of pit morphology between potentiostatically and galvanostatically grown pits is likely to be a result of the decrease in interfacial potential during the course of galvanostatic pit growth.

4.2. Current density around pit perimeter and its variation with time

The approach presented here and in a previous publication [41] shows how the local current density around the perimeter of a pit can be quantified. Previous work of Ernst and Newman [11,12] showed the overall change of pit shape with time, but there was no quantification of local current density. Other researchers have measured the average values from circular pits growing in thin films, and so have not captured the difference in current density that arises locally from the escape of metal ions from the pit mouth. There have been a number of purely electrochemical measurements of pit current density made on the basis of assuming that pits grow homogeneously as hemispheres: the current density values vary in the rage of 0.1–10 A/cm^2 for metastable pits [8,9,54] and stable pits [52,55]. Similar average values are found in the present work, but the key novel contribution of this paper is the quantification of the variation of local current density around the perimeter of the pit.

For pits under potentiostatic control, the pit current densities can be divided into three regions, consistent with those used in the model of Laycock and co-workers [14]. Near the mouth of the pit, where the concentration of metal ions in the solution is relatively low, the metal repassivates, leading to a negligible current density. At the bottom of the pit, where the presence of a salt layer is expected, typical current densities are in the range of 1–2 A/cm^2. Higher current densities, in the range of 3–5 A/cm^2 are found between the passive and salt layer regions where pit lobes grow laterally with active dissolution in the absence of any salt layer. Close to the pit mouth, there is a remarkably sharp transition between the high active dissolution and the adjacent passive region. The high current density characteristic of this transition may relate to the critical current density for passivation, i_{crit}, proposed by Salinas-Bravo and Newman [56], a concept that has been recently further developed [57–60]. The observation of an extremely sharp transition between active and passive regions may also shed light on mechanisms of stress corrosion cracking (SCC) that require passive walls and an active tip to maintain the conditions necessary for transgranular SCC.

The current density trend in all potentiostatically grown pits shown in Fig. 12 indicates that the maximum i_a fluctuates around a certain value which slightly decreases as the pits grow. Less fluctuation is seen in mid-point current density which can be considered as the current density at the pit bottom (assuming symmetrical pit shape) and there is a smooth decrease during pit growth.

Comparing the maximum current densities associated with lateral growth (i_a) shown in Fig. 14 shows that an increase in the chloride concentration of the bulk solution results in slightly higher current density. This result suggests a dependence of the growth rate at laterally developing lobes on bulk chloride concentration, and in particular to the resulting *IR* drop associated with the solution. In other words, the growth rate at developing lobes (where i_a is at its maximum) depends on the interfacial potential, therefore an increase in the chloride concentration in the bulk solution causes a smaller *IR* drop and thus a higher interfacial potential, which leads to higher dissolution rate and i_a. The dependence of lateral growth on potential supports the idea that the lateral corroding surface is not covered with a salt layer which is consistent with the observations of Ryan et al. [27,36] and Ernst and Newman [11].

The current density profiles shown in Fig. 13 illustrate a clear decrease with growth time which is a characteristic of galvanostatic growth, in which, as the pit propagates and corroding surface increases, the local current density reduces due to the limited availability of applied current. Additionally, as the pit propagates, a more uniform distribution of current within the pit can be deduced from the smaller difference between the maximum and pit mid-point current density, indicating a stabilisation of its characteristic aspect ratio (i.e. the ratio between width and depth) after an initial transient. The decrease in current density with time is consistent with the observations of Alkire and Wong [52], although in our work a linear relationship between current density and the square root of time was not observed.

4.3. Growth of pit depth

In this work, a linear relationship has been observed between the square of the pit depth (h^2) and time (t), consistent with diffusion-controlled growth [20,23,53,61–65]. The gradient of h^2 vs. t plots is proportional to the product $D_{eff}\Delta C$, which is given in Table 2. This suggests that pits grow in depth under diffusion control. Although the slopes ($D_{eff}\Delta C$ values) showed some variability (generally within a factor of 2), no systematic change was found with chloride concentration, or even if the pits are grown under potentiostatic or galvanostatic control. This supports the idea that stable pits grow under diffusion control with a salt layer at the bottom, which adjusts in thickness so that the interfacial potential between the metal and the salt layer gives a current density equal to the rate of diffusion of metal ions [26,61] As a result, the growth of pit depth depends only marginally on the external conditions (both polarisation and chloride concentration).

While it would be expected that $D_{eff}\Delta C$ may depend to some extent upon the pit geometry, the most likely cause of the variation is likely to be the (unknown) variation in the extent of pit cover perforation developed in different conditions. If no cover exists (a condition achieved in the case of the '1D' pit in this study), a maximum $D_{eff}\Delta C$ is likely to be observed. In this study the 1D pit value of $D_{eff}\Delta C$ is in broad agreement with the values reported in the literature (Table 1). The decrease in $D_{eff}\Delta C$ obtained for pits with a (perforated) cover (typically 50% of the maximum value) can be attributed to the decrease in the rate of effective diffusion of metal ions away from the pit provided by such physical barrier.

The variation in perforation factor in pit growth is a major source of uncertainty in the prediction of pit growth. Its role in pit stability is important, acting either as a resistive barrier [9] or a diffusion barrier [8], thus protecting metastable pits and even stable pits [4,6] from repassivation. In order to provide useful input parameters for insertion into pit growth models, the simplest approach suggested in this work is to estimate an empirically determined "perforation

factor" by taking the ratio of the value for a 'covered' pit with the value obtained for a pit without a cover.

4.4. Lateral growth of pits

As shown in Figs. 19 and 20, the pit width growth rate increases with chloride concentration. These changes are consistent with the results of Ernst and Newman [11]. The most likely reason for the changes in width with chloride concentration is that an increase in the bulk chloride concentration leads to a decrease in IR drop in the solution and therefore, an increase in the interfacial potential and dissolution rate at the laterally developing fronts, which grow under activation/ohmic-drop control. However, at the pit bottom, dissolution is diffusion-limited as described above, so that changes in the pit depth with time are independent of salt concentration.

Comparison of pits that have grown under potentiostatic or galvanostatic control in solutions of the same chloride concentration show that while the pit depths are similar (growing under diffusion control), the pit widths are greater for the pits grown under potentiostatic control. This can be attributed to the lower potential measured during the galvanostatic experiments carried out in this work.

4.5. Pit stability

Fig. 22(a) shows that the pit at the initial stages grows below the stability product of 2.5 mA/cm. This is in agreement with the work of Pistorius and Burstein [8] which showed that metastable and even stable pits initially grew with the stability products value below 3 mA/cm. This is due to the diffusion barrier provided by the pit cover, as is visible in the figure, which maintains the concentrated solution inside pit cavity. Fig. 22(b) shows the slight increase in the stability product as the pit enlarges. The stability products as a function of time for galvanostatically grown pits, shown in Fig. 23, illustrate an initial increase, but tend to fluctuate between 3 and 4 mA/cm for the rest of growth time. It is seen that pits initially grow below the stability product with the support of their cover. Even after that, only at the pit bottom does the stability product exceed 3 mA/cm; the rest of boundary grows under conditions below the stability value because of diffusion barrier provided by cover. This emphasises the importance of the lacy cover for transport of metal ions from the pit bottom into the bulk solution and supports the proposed "*perforation factor*".

5. Conclusions

1. Radiography observations have confirmed that the pits grown under potentiostatic control at relatively high potentials develop via lobes through an undercutting process that perforates the metal surface and gradually changes the pit shape from semi-circular at the start to dish-shaped as growth occurs. In these conditions, the pit perimeter is smooth, consistent with the presence of stable chemical conditions (and hence propagation rates) within the pit (the salt layer present at the pit bottom is likely to provide a chemical buffer to any externally driven change).
2. In the early stages of pit growth under galvanostatic control following initiation under potentiostatic control, pits propagate by lobes undercutting the metal in a similar way to potentiostatic growth. As the pits propagate under constant current, however, the potential decreases and they tend to approach a circular shape with a rough etched surface at the bottom, which is likely to grow close to the critical concentration required for propagation, without a salt layer. The change in growth mode may also be associated with a result of the gradual decrease in potential as the pit grows.
3. The local current density along pit perimeter can be directly measured from the movement of the pit boundary with suitable imaging techniques (e.g. X-ray radiography). The active local current density inferred on the basis of these techniques varied (locally) between ~1 and 5 A/cm^2.
4. The maximum current density along the pit perimeter is observed at the transition point from the passive to active region of the pit wall and is between ~3 and 5 A/cm^2. It is suggested that this is the critical passivation current density, i_{crit}, which increases slightly with increase in the bulk chloride concentration. The lowest active current density is seen at the pit bottom, and is a diffusion-limited current density associated with a metal-chloride salt layer.
5. The current density within a pit under potentiostatic control remains almost constant during growth, whereas it shows significant decrease during galvanostatic pit growth.
6. For both potentiostatically and galvanostatically grown pits, a linear relation exists between the square of the pit depth and growth time, and is independent of the bulk chloride concentration, which suggests that increase in pit depth is under diffusion control, and the pit bottom is covered with a salt layer.
7. The diffusion-related parameter $D_{eff}\Delta C$ can be extracted from the radiographic 2D pit growth data and found to vary around 50% of the value for a 1D pit reflecting the effectiveness of lacy pit covers in hindering diffusion of metal ions from the pit. The value increases with increasing chloride concentration of the bulk solution, reflecting the increase in porosity of the cover.
8. Lateral growth of pits is controlled by the conductivity (and therefore chloride concentration) in the solution for both potential- and current-controlled regimes.

Acknowledgments

This work was supported by the UK Nuclear Decommissioning Authority under contracts NR 3331 and NR 3274, and by the New Zealand Foundation for Research Science and Technology under contract 8X0409, and by EPSRC grant EP/E045464/1. Fast radiography measurements were carried out at the TOMCAT beamline at the Swiss Light Source.

References

[1] O.E. Albores-Silva, E.A. Charles, C. Padovani, Effect of chloride deposition on stress corrosion cracking of 316L stainless steel used for intermediate level radioactive waste containers, Corros. Eng. Sci. Technol. 46 (2011).
[2] Nuclear Decommissioning Authority, Geological Disposal: Package Evolution Status Report, NDA/RWMD/031, 2010 www.nda.gov/documents/biblio
[3] W. Schwenk, Theory of stainless steel pitting, Corrosion 20 (1964) 129t–137t.
[4] I.L. Rosenfeld, I.S. Danilov, Electrochemical aspects of pitting corrosion, Corros. Sci. 7 (1967) 129–142.
[5] H.W. Pickering, R.P. Frankenthal, Mechanism of localized corrosion of iron and stainless-steel. 2. Morphological studies, J. Electrochem. Soc. 119 (1972) 1304–1310.
[6] H.S. Isaacs, G. Kissel, Surface preparation and pit propagation in stainless-steels, J. Electrochem. Soc. 119 (1972) 1628–1632.
[7] J. Mankowski, Z. Szklarska-Smialowska, Studies on accumulation of chloride-ions in pits growing during anodic polarization, Corros. Sci. 15 (1975) 493–501.
[8] P.C. Pistorius, G.T. Burstein, Metastable pitting corrosion of stainless-steel and the transition to stability, Philos. Trans. R. Soc. Lond. Ser. A-Math. Phys. Eng. Sci. 341 (1992) 531–559.
[9] G.S. Frankel, L. Stockert, F. Hunkeler, H. Boehni, Metastable pitting of stainless-steel, Corrosion 43 (1987) 429–436.
[10] P. Ernst, N.J. Laycock, M.H. Moayed, R.C. Newman, The mechanism of lacy cover formation in pitting, Corros. Sci. 39 (1997) 1133–1136.
[11] P. Ernst, R.C. Newman, Pit growth studies in stainless steel foils. I. Introduction and pit growth kinetics, Corros. Sci. 44 (2002) 927–941.
[12] P. Ernst, R.C. Newman, Pit growth studies in stainless steel foils. II. Effect of temperature, chloride concentration and sulfate addition, Corros. Sci. 44 (2002) 943–954.
[13] S.M. Ghahari, A.J. Davenport, T. Rayment, T. Suter, J.-P. Tinnes, C. Padovani, J.A. Hammons, M. Stampanoni, F. Marone, R. Mokso, In situ synchrotron X-ray

micro-tomography study of pitting corrosion in stainless steel, Corros. Sci. 53 (2011) 2684–2687.
[14] N.J. Laycock, S.P. White, Computer simulation of single pit propagation in stainless steel under potentiostatic control, J. Electrochem. Soc. 148 (2001) B264–B275.
[15] N.J. Laycock, S.P. White, W. Kissling, The shape of pits in stainless, in: M. Seo, B. Macdougall, H. Takahashi, R.G. Kelly (Eds.), Passivity and Localized Corrosion: An International Symposium in Honour of Norio Sato, PV 99-27, The Electrochemical Society Proceedings Series, Pennington, NJ, USA, 1999, p. 541.
[16] N.J. Laycock, S.P. White, J.S. Noh, P.T. Wilson, R.C. Newman, Perforated covers for propagating pits, J. Electrochem. Soc. 145 (1998) 1101–1108.
[17] N.J. Laycock, S.P. White, A Model for Pit Propagation in Stainless Steels, Electrochemical Society Inc, Pennington, 1999.
[18] J.R. Galvele, Transport processes and mechanism of pitting of metals, J. Electrochem. Soc. 123 (1976) 464–474.
[19] D.E. Williams, J. Stewart, P.H. Balkwill, The nucleation, growth and stability of micropits in stainless steel, Corros. Sci. 36 (1994) 1213–1235.
[20] H.C. Kuo, D. Landolt, Rotating-disk electrode study of anodic dissolution or iron in concentrated chloride media, Electrochim. Acta 20 (1975) 393–399.
[21] G.T. Gaudet, W.T. Mo, T.A. Hatton, J.W. Tester, J. Tilly, H.S. Isaacs, R.C. Newman, Mass-transfer and electrochemical kinetic interactions in localized pitting corrosion, AlChE J. 32 (1986) 949–958.
[22] U. Steinsmo, H.S. Isaacs, Dissolution and repassivation kinetics of Fe–Cr alloys in pit solutions. 1. Effect of the surface salt layer, J. Electrochem. Soc. 140 (1993) 643–653.
[23] J.W. Tester, H.S. Isaacs, Diffusional effects in simulated localized corrosion, J. Electrochem. Soc. 122 (1975) 1438–1445.
[24] T.R. Beck, R.C. Alkire, Occurrence of salt films during initiation and growth of corrosion pits, J. Electrochem. Soc. 126 (1979) 1662–1666.
[25] D. Landolt, Mass-transport processes in anodic metal dissolution, Russ. J. Electrochem. 31 (1995) 206–211.
[26] N.J. Laycock, R.C. Newman, Localised dissolution kinetics, salt films and pitting potentials, Corros. Sci. 39 (1997) 1771–1790.
[27] M.P. Ryan, N.J. Laycock, H.S. Isaacs, R.C. Newman, Corrosion pits in thin films of stainless steel, J. Electrochem. Soc. 146 (1999) 91–97.
[28] A.G. Carcea, E.Y.W. Yip, D.D. He, R.C. Newman, Anodic kinetics of NiCr Mo alloys during localized corrosion: I. diffusion-controlled dissolution, J. Electrochem. Soc. 158 (2011) C215–C220.
[29] T. Rayment, A.J. Davenport, A.J. Dent, J.P. Tinnes, R.J.K. Wiltshire, C. Martin, G. Clark, P. Quinn, J.F.W. Mosselmans, Characterisation of salt films on dissolving metal surfaces in artificial corrosion pits via in situ synchrotron X-ray diffraction, Electrochem. Commun. 10 (2008) 855–858.
[30] H.S. Isaacs, J.H. Cho, M.L. Rivers, S.R. Sutton, In-situ X-ray microprobe study of salt layers during anodic-dissolution of stainless-steel in chloride solution, J. Electrochem. Soc. 142 (1995) 1111–1118.
[31] F. Hunkeler, H. Bohni, Mass-transport-controlled pit growth on stainless steels and nickel, in: A. Turnbull (Ed.), Corrosion Chemistry in Pits, Crevices and Cracks, HMSO, London, 1987.
[32] J. Enerhaug, U.M. Steinsmo, O. Grong, L.R. Hellevik, Dissolution and repassivation kinetics of a 12.3Cr–2.6Mo–6.5Ni super martensitic stainless steel – a comparative study, J. Electrochem. Soc. 149 (2002) B256–B264.
[33] G.S. Frankel, The growth of 2-d pits in thin-film aluminium, Corros. Sci. 30 (1990) 1203–1218.
[34] G.S. Frankel, R.C. Newman, C.V. Jahnes, M.A. Russak, On the pitting resistance of sputter-deposited aluminium-alloys, J. Electrochem. Soc. 140 (1993) 2192–2197.
[35] G.S. Frankel, J.O. Dukovic, V. Brusic, B.M. Rush, C.V. Jahnes, Pit growth in NiFe thin-films, J. Electrochem. Soc. 139 (1992) 2196–2201.
[36] M.P. Ryan, N.J. Laycock, R.C. Newman, H.S. Isaacs, The pitting behavior of iron-chromium thin film alloys in hydrochloric acid, J. Electrochem. Soc. 145 (1998) 1566–1571.
[37] P. Ernst, M.H. Moayed, N.J. Laycock, R.C. Newman, Shape of Corrosion Pits in Metals, in: P. Schmuki, D.J. Lockwood, Y.H. Ogata, H.S. Isaacs, A. Bsiesy (Eds.), Proceedings of the International Symposium on Pits and Pores: Formation, Properties, and Significance for Advanced Luminescent Materials Electrochemical Society, Corrosion Division, Electrochemical Society, Montreal, 1997, pp. 176–185.
[38] Y.C. Tang, A.J. Davenport, Magnetic field effects on the corrosion of artificial pit electrodes and pits in thin films, J. Electrochem. Soc. 154 (2007) C362–C370.
[39] D. Krouse, N. Laycock, C. Padovani, Modelling pitting corrosion of stainless steel in atmospheric exposures to chloride containing environments, Corros. Eng. Sci. Technol. 49 (2014) 521–528.
[40] A.J. Davenport, L. Guo, N. Mi, H. Mohammed-Ali, M. Ghahari, S.R. Street, N. Laycock, T. Rayment, C. Reinhard, C. Padovani, D. Krouse, Mechanistic studies of atmospheric pitting corrosion of stainless steel for ILW containers, Corros. Eng. Sci. Technol. 49 (2014) 514–520.
[41] S.M. Ghahari, D.P. Krouse, N.J. Laycock, T. Rayment, C. Padovani, T. Suter, R. Mokso, F. Marone, M. Stampanoni, M. Monir, A.J. Davenport, Pitting corrosion of stainless steel: measuring and modelling pit propagation in support of damage prediction for radioactive waste containers, Corros. Eng. Sci. Technol. 46 (2011) 205–211.
[42] F. Hunkeler, H. Bohni, The significance of pit induction times, Corrosion 40 (1984) 559–560.
[43] W.S. Rasband, ImageJ, in: U.S. National Institutes of Health, Bethesda, Maryland, USA, 1997.
[44] S.M. Ghahari, In situ synchrotron X-ray characterisation and modelling of pitting corrosion of stainless steel, in: Metallurgy and Materials, University of Birmingham, Birmingham, 2012.
[45] J. Yahalom, L.K. Ives, J. Kruger, Nature of films over corrosion pits in stainless-steel, J. Electrochem. Soc. 120 (1973) 384–386.
[46] C. Punckt, M. Bolscher, H.H. Rotermund, A.S. Mikhailov, L. Organ, N. Budiansky, J.R. Scully, J.L. Hudson, Sudden onset of pitting corrosion on stainless steel as a critical phenomenon, Science 305 (2004) 1133–1136.
[47] J.R. Scully, N.D. Budiansky, Y. Tiwary, A.S. Mikhailov, J.L. Hudson, An alternate explanation for the abrupt current increase at the pitting potential, Corros. Sci. 50 (2008) 316–324.
[48] M.I. Suleiman, R.C. Newman, The use of very weak galvanostatic polarization to study localized corrosion stability in stainless-steel, Corros. Sci. 36 (1994) 1657–1665.
[49] D.P. Krouse, P. McGavin, N.J. Laycock, Computer simulation of pitting corrosion: multiple interacting pits, in: Corrosion & Prevention Australian Corrosion Association, Wellington, 2008.
[50] N. Sato, The stability of localized corrosion, Corros. Sci. 37 (1995) 1947–1967.
[51] N. Sato, The stability of pitting dissolution of metals in aqueous-solution, J. Electrochem. Soc. 129 (1982) 260–264.
[52] R.C. Alkire, K.P. Wong, The corrosion of single pits on stainless-steel in acidic chloride solution, Corros. Sci. 28 (1988) 411–421.
[53] A.J. Davenport et al., unpublished work (2010).
[54] H. Ezuber, R.C. Newman, Growth-rate distribution of metastable pits, in: G.S. Frankel, R.C. Newman (Eds.), Critical Factors in Localized Corrosion, The Electrochemical Society, Pennington, NJ, 1992.
[55] H.W. Pickering, R.P. Frankenthal, Mechanism of localized corrosion of iron and stainless-steel. 1. Electrochemical studies, J. Electrochem. Soc. 119 (1972) 1297–1304.
[56] V.M. Salinas-Bravo, R.C. Newman, An alternative method to determine critical pitting temperature of stainless steels in ferric chloride solution, Corros. Sci. 36 (1994) 67–77.
[57] N.J. Laycock, M.H. Moayed, R.C. Newman, Metastable pitting and the critical pitting temperature, J. Electrochem. Soc. 145 (1998) 2622–2628.
[58] M.H. Moayed, N.J. Laycock, R.C. Newman, Dependence of the critical pitting temperature on surface roughness, Corros. Sci. 45 (2003) 1203–1216.
[59] M.H. Moayed, R.C. Newman, The relationship between pit chemistry and pit geometry near the critical pitting temperature, J. Electrochem. Soc. 153 (2006) B330–B335.
[60] M.H. Moayed, R.C. Newman, Deterioration in critical pitting temperature of 904L stainless steel by addition of sulfate ions, Corros. Sci. 48 (2006) 3513–3530.
[61] H.S. Isaacs, Behavior of resistive layers in localized corrosion of stainless-steel, J. Electrochem. Soc. 120 (1973) 1456–1462.
[62] A.C. West, R.D. Grimm, D. Landolt, C. Deslouis, B. Tribollet, Electrohydrodynamic impedance study of anodically formed salt films on iron in chloride solutions, J. Electroanal. Chem. 330 (1992) 693–706.
[63] R.D. Grimm, D. Landolt, Salt films formed during mass-transport controlled dissolution of iron-chromium alloys in concentrated chloride media, Corros. Sci. 36 (1994) 1847–1868.
[64] R.D. Grimm, A.C. West, D. Landolt, AC impedance study of anodically formed salt films on iron in chloride solution, J. Electrochem. Soc. 139 (1992) 1622–1629.
[65] F. Hunkeler, A. Krolikowski, H. Bohni, A study of the solid salt film on nickel and stainless-steel, Electrochim. Acta 32 (1987) 615–620.